WIDETECT: A ROBUST AND LOW-COMPLEXITY WIRELESS MOTION DETECTOR

Feng Zhang[⋆†], *Chen Chen*[⋆†], *Beibei Wang*[⋆†*], *Hung-Quoc Lai*[⋆*], *Yi Han*[⋆*] *and K. J. Ray Liu*[⋆†]

[†]University of Maryland, College Park, MD 20742, USA.
[⋆]Origin Wireless Inc., 7500 Greenway Center Drive, Suite 1070, MD 20770, USA.
Email: {fzhang15, cc8834, kjrliu}@umd.edu[†], {beibei.wang, quoc.lai, yi.han}@originwireless.net[*]

ABSTRACT

Motion detection as a key component in modern security systems has received an increasing attention recently, but most existing solutions require special installation, calibration, and only have a limited coverage. In this paper, we propose WiDetect, a highly accurate, calibration-free, and low-complexity wireless motion detector. By exploiting the statistical theory of electromagnetic waves, we establish a link between the autocorrelation function of the physical layer channel state information (CSI) and motion in the environment. Temporal, frequency and spatial diversity are also exploited to further improve the robustness and accuracy of WiDetect. Extensive experiments conducted in several facilities show that WiDetect can achieve similar detection performance compared to a commercial home security system, while with much larger coverage and lower cost.

Index Terms— Wireless sensing, motion detection, statistical theory

1. INTRODUCTION

Motion detection plays a vital role in modern security systems. However, popular approaches that rely on video, infrared, RFID, UWB, etc. all require specialized hardware deployment and has its own limitation in practical applications. For example, the vision-based schemes [1] can only perform motion monitoring in areas covered by camera, and in addition they introduce privacy issues. The infrared-based motion sensors are especially sensitive to thermal radiation, leading to high false alarm rate.

Recently, WiFi has been considered in wireless sensing due to its deployment flexibility, large coverage, and cost efficiency. RASID [2] is exploits the fluctuations of the receive signal strength indicator (RSSI) to detect the presence of human in indoors, based on the dissimilarity in RSSI distribution in a static environment. E-eyes [3] follows a similar idea but uses CSI instead of RSSI as the metric. PILOT [4] decomposes the CSI amplitude correlation matrix using singular value decomposition (SVD) and monitors the variations of the singular vectors along time. Similarly, CARM [5] tracks the variance of the second singular vector to detect motion. WiDar [6] computes cross-correlation among different subcarriers and uses the increase in the correlation between adjacent subcarriers as an indicator of motion. Table 1 summarizes the performance of most existing approaches, where the second column shows the false negative and false positive rate and the third column shows whether calibration is needed. As can be seen, all of them rely on some kind of calibration before use, such as storing the features of normal states, or fine-tuning of parameters, which is not robust to the environmental dynamics and not easy to use for ordinary users. Also, their performance in terms of coverage, accuracy, and computational complexity, is quite far from meeting the requirement of real applications.

Table 1. Related Works

Reference	FN/FP	Cal.
RASID [2]	$3.8\%/4.7\%$	Yes
PILOT [4]	$10.0\%/10.0\%$	Yes
E-eyes [3]	$10.0\%/1.0\%$	Yes
Omni-PHD [7]	$8.0\%/7.0\%$	Yes
DeMan [8]	$5.93\%/1.45\%$	Yes
CARM [5]	$2.0\%/1.4$ times per hour	Yes
SIED [9]	$0\%/6.4\%$(slow motion)	Yes

To address these challenges, in this paper, we present WiDetect, a highly accurate and robust WiFi-based motion detector that can cover a large area and is easy to use. We first characterize the impact of motion on the autocorrelation function (ACF) of the received channel power response using statistical theory of electromagnetic (EM) waves. Then, we define a *motion statistic* to measure the likelihood of the presence of motion. To improve the accuracy of detection, WiDetect combines all the motion statistics obtained from multiple subcarriers, and the impact of the number of CSI measurements and the number of available subcarriers on WiDetect is quantified. We conduct extensive experiments in an office and a single family home, where 4 PIRs are deployed for comparison. Experiment results show that WiDetect is able to detect human motion in a large area while maintaining a negligible false alarm rate.

The rest of the paper is organized as follows. Section 2 presents a statistical modeling of the CSI measurements based on statistical theory of EM waves. The detailed design of WiDetect is presented in Section 3 and experimental evaluation is discussed in Section 4. Section 5 concludes the paper.

2. STATISTICAL MODELING OF CSI MEASUREMENTS

In this section, we discuss the theoretical basis of WiDetect.

2.1. CSI Measurement

Consider a pair of WiFi devices deployed in an indoor environment and the transmitter (Tx) keeps transmitting signals to the receiver (Rx). Let $X(t,f)$ and $Y(t,f)$ be the transmitted and received signals over a subcarrier with frequency f at time t. Then, the CSI on the subcarrier with frequency f at time t is $H(t,f) = \frac{Y(t,f)}{X(t,f)}$ [10], which is a complex number and can be obtained from the PHY layer of commercial WiFi. However, in practice, the estimated $H(t,f)$ often suffers from severe phase distortions [11, 12], so in this work we only use the magnitude of $H(t,f)$ and define the power response of the CSI $G(t,f)$ as follows,

$$G(t,f) \triangleq |H(t,f)|^2 = \mu(t,f) + \varepsilon(t,f), \tag{1}$$

where $\mu(t,f)$ denotes the part contributed by the propagations of the EM waves, and $\varepsilon(t,f)$ denotes the measurement noise. Let $\mathcal{F}$ denote the set of available subcarriers. For any given subcarrier $f \in \mathcal{F}$, $\varepsilon(t,f)$ can be shown through experiment measurements to be an additive white Gaussian noise, i.e., $\varepsilon(t,f) \sim \mathcal{N}(0, \sigma^2(f))$, and $\varepsilon(t_1,f_1)$ and $\varepsilon(t_2,f_2)$ are independent for any two different subcarriers $f_1 \neq f_2$ or any two different time slots $t_1 \neq t_2$.

2.2. Modeling of the Signal Term

Radio propagation in a building interior is in general very difficult to analyze because the EM waves can be absorbed and scattered by walls, doors, windows, moving objects, etc. However, buildings and rooms can be viewed as reverberation cavities in that they exhibit internal multipath propagations. Hence, we refer to a statistical modeling instead of a deterministic one and apply the statistical theory of EM fields developed for reverberation cavities to analyze the statistical properties of the signal term $\mu(t,f)$.

Consider a rich-scattering environment as illustrated in Fig. 1, which is typical for indoor spaces. The scatterers are assumed to be diffusive and can reflect the impinging EM waves towards all directions. A pair of Tx and Rx are deployed in the environment, both equipped with omnidirectional antennas, and the Tx emits a continuous EM wave via its antennas, which is received by

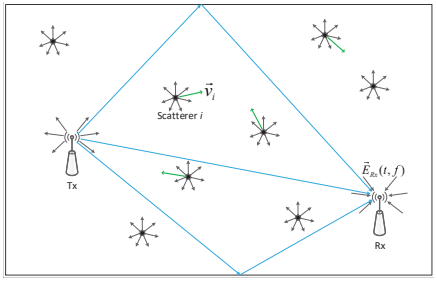

Fig. 1. Propagation of radio signals in scattering environment.

the Rx and the corresponding received electric field is denoted as $\vec{E}_{Rx}(t,f)$. Actually, $\mu(t,f)$ measures the power of $\vec{E}_{Rx}$, i.e., $\mu(t,f) = \|\vec{E}_{Rx}(t,f)\|^2$, where $\|\cdot\|^2$ denotes the Euclidean norm. Within a sufficiently short period, $\vec{E}_{Rx}(t,f)$ can be decomposed into two parts as $\vec{E}_{Rx}(t,f) \approx \vec{E}_s(f) + \sum_{i\in\Omega_d} \vec{E}_i(t,f)$, where $\vec{E}_s(f)$ and $\vec{E}_i(t,f)$ denote the components contributed by all the static scatterers and the i-th dynamic scatterer, respectively, and Ω_d denotes the set of dynamic scatterers in the environment. When the environment is static, Ω_d is empty. The intuition behind the decomposition is that each scatterer can be treated as a "virtual antenna" diffusing the received EM waves in all directions and then these EM waves add up together at the receive antenna after bouncing off the walls, ceilings, furniture, windows, etc. of the building.

Let v_i denote the speed of the i-th moving scatterer and $\vec{E}_i(t,f)$ is expanded in the orthogonal basis as $\vec{E}_i(t,f) = E_{i,x}(t,f)\hat{x} + E_{i,y}(t,f)\hat{y} + E_{i,z}(t,f)\hat{z}$, where $E_{i,u}(t,f)$ denotes the linear component of $\vec{E}_i(t,f)$ along the direction $\hat{u}$, $u \in \{x, y, z\}$, and $\hat{z}$ points to the moving direction of the scatterer. Then, under certain common assumptions on the homogeneity of scattering for reverberation cavities [13], the ACF for each linear component of $\vec{E}_i(t,f)$ can be derived in closed forms as

$$\begin{aligned}\rho_{E_{i,x}}(\tau,f) &= \rho_{E_{i,y}}(\tau,f) \\ &= \frac{3}{2}\left[\frac{\sin(kv_i\tau)}{kv_i\tau} - \frac{1}{(kv_i\tau)^2}\left(\frac{\sin(kv_i\tau)}{kv_i\tau} - \cos(kv_i\tau)\right)\right], \quad (2)\end{aligned}$$

$$\rho_{E_{i,z}}(\tau,f) = \frac{3}{(kv_i\tau)^2}\left[\frac{\sin(kv_i\tau)}{kv_i\tau} - \cos(kv_i\tau)\right], \quad (3)$$

where k is the wave number of the transmitted signal and τ denotes the time lag. Denote $E_i^2(f)$ as the radiation power of the i-th scatterer, $E_d^2(f)$ as the variance of $\mu(t,f)$, and assume that $\vec{E}_{i_1}(t,f)$ and $\vec{E}_{i_2}(t,f)$ are statistically uncorrelated for $\forall i_1 \neq i_2$, the ACF of $\mu(t,f)$ can be approximated as

$$\begin{aligned}\rho_\mu(\tau,f) \approx \frac{1}{E_d^2(f)} \sum_{u\in\{x,y,z\}} \Bigg(&\sum_{i\in\Omega_d} \frac{2E_{s,u}^2(f)E_i^2(f)}{3}\rho_{E_{i,u}}(\tau,f) \\ &+ \sum_{\substack{i_1,i_2\in\Omega_d \\ i_1\geq i_2}} \frac{E_{i_1}^2(f)E_{i_2}^2(f)}{9}\rho_{E_{i_1,u}}(\tau,f)\rho_{E_{i_2,u}}(\tau,f)\Bigg). \quad (4)\end{aligned}$$

An important observation is that when $\tau \to 0$, $\rho_\mu(\tau, f) \to 1$.

2.3. Modeling of the CSI Power Response

As $\mu(t, f)$ is due to the propagations of EM waves and $\varepsilon(t, f)$ is due to the imperfect measurements of CSI, it can be shown through experimental results that $\mu(t, f)$ and $\varepsilon(t, f)$ are uncorrelated with each other, i.e., $\mathrm{cov}(\mu(t_1, f), \varepsilon(t_2, f)) = 0$, for $\forall t_1$, t_2, Therefore, the auto-covariance function of $G(t, f)$ can be expressed as

$$\begin{aligned}\gamma_G(\tau, f) &\triangleq \mathrm{cov}\Big(\mu(t, f)+\varepsilon(t, f), \mu(t-\tau, f)+\varepsilon(t-\tau, f)\Big) \\ &= E_d^2(f)\rho_\mu(\tau, f)+\sigma^2(f)\delta(\tau), \end{aligned} \tag{5}$$

where $\delta(\cdot)$ is Dirac delta function. The corresponding ACF of $G(t, f)$ can thus be expressed as

$$\rho_G(\tau, f) = \frac{E_d^2(f)}{E_d^2(f) + \sigma^2(f)}\rho_\mu(\tau, f), \tag{6}$$

where $\tau \neq 0$. When there exists motion and $\tau \to 0$, with the knowledge of $\rho_\mu(\tau, f) \to 1$, we know $\rho_G(\tau, f) \to \frac{E_d^2(f)}{E_d^2(f)+\sigma^2(f)} > 0$; when there is no motion and $\tau \to 0$, we have $\rho_G(\tau, f) = 0$ since $E_d^2(f) = 0$. Therefore, $\lim_{\tau\to 0} \rho_G(\tau, f)$ is a good indicator of the presence of motion, which is only determined by $E_d^2(f)$ incurred by motion and the power of the measurement noise $\sigma^2(f)$. We will exploit this important observation in the following design of WiDetect.

3. DESIGN OF WIDETECT

In this section, we propose the motion statistics and the detection rule, and analyze the performance of WiDetect.

3.1. Motion Statistics

In practice, $\lim_{\tau\to 0} \rho_G(\tau, f)$ cannot be measured directly, because $\tau \to 0$ is difficult to achieve due to finite channel sampling rate F_s. Instead, we use the quantity $\rho_G\Big(\tau = \frac{1}{F_s}, f\Big)$ as an approximation as long as F_s is large enough. Then, we define the *motion statistic* from the CSI power response $G(t, f)$ as the sample ACF of $G(t, f)$,

$$\hat{\phi}(f) = \frac{\hat{\gamma}_G\Big(\tau = \frac{1}{F_s}, f\Big)}{\hat{\gamma}_G(\tau = 0, f)}, \tag{7}$$

where $\hat{\gamma}_G(\tau, f)$ denotes the sample auto-covariance function of $G(t, f)$ [14]. When there is no motion, according to the large sample theory [14], the distribution of $\hat{\phi}(f)$ will converge to an asymptotically normal (AN) distribution with mean $-\frac{1}{T}$ and variance $\frac{1}{T}$ as T approaches infinity, i.e., $\hat{\phi}(f) \sim \mathcal{AN}(-\frac{1}{T}, \frac{1}{T})$ as $T \to \infty$, with T as the number of samples. In addition, $\hat{\phi}(f_1)$ and $\hat{\phi}(f_2)$ are i.i.d. for $\forall f_1 \neq f_2$. When there exists motion, $\hat{\phi}(f)$ will converge to a positive constant $\frac{E_d^2(f)}{E_d^2(f)+\sigma^2(f)}$ as $F_s \to \infty$ and $T \to \infty$.

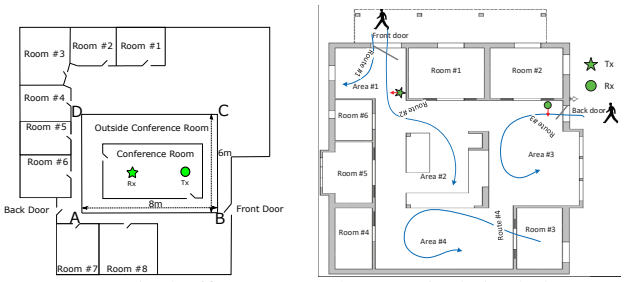

(a) A typical office. (b) A typical single house.

Fig. 2. Floorplans of two different environments.

3.2. Detection Rule

In order to improve the reliability of WiDetect, the motion statistics obtained from all the available subcarriers can be combined together. In this paper we define the aggregated motion statistics as the average of all the individual motion statistics, i.e., $\hat{\psi} = \frac{1}{F}\sum_{f\in\mathcal{F}} \hat{\phi}(f)$. We know that when there is no motion, $\hat{\phi}(f)$ converges to an AN distribution and $\hat{\phi}(f_1)$ and $\hat{\phi}(f_2)$ are i.i.d. for $\forall f_1 \neq f_2$. Therefore, the distribution of $\hat{\psi}$ can be approximated as $\hat{\psi} \sim \mathcal{AN}(-\frac{1}{T}, \frac{1}{FT})$. Since the variance of $\hat{\psi}$ is inversely proportional to the number of samples T and the number of subcarriers F, increasing T and F will improve the detection performance.

According to the above analysis, a simple detection rule is proposed: *WiDetect detects motion only if* $\hat{\psi} \geq \eta$. Given a preset threshold η, the probability of false alarm can be approximated as

$$P(\hat{\psi} \geq \eta) \approx Q\Big(\sqrt{FT}(\eta + \frac{1}{T})\Big), \tag{8}$$

where $Q(\cdot)$ denotes the tail probability of the standard normal distribution, i.e., $Q(x) = \frac{1}{2\pi}\int_x^\infty \exp(-\frac{u^2}{2})\,\mathrm{d}u$.

4. EXPERIMENTAL EVALUATION

To evaluate the performance of WiDetect, a prototype based on a pair of commercial WiFi devices is built to detect human motion in two different environments as shown in Fig. 2. The carrier frequency is set to 5.805 GHz, and the channel sampling rate is 30 Hz. Each WiFi device is equipped with 3 omnidirectional antennas, and each antenna-pair link has a total of 114 subcarriers. To avoid the correlations among adjacent subcarriers, we take one subcarrier from every two adjacent ones and only use 58 subcarriers for each link, considering the fact that the CSI of DC subcarrier is not accessible.

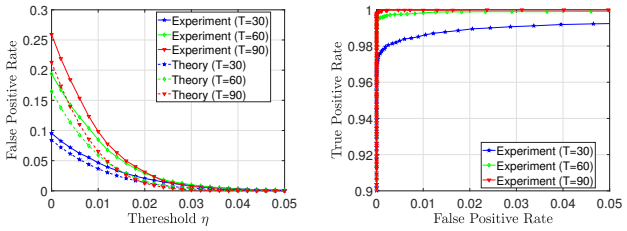

(a) False positive rate ($F = 58$). (b) ROC for varying T.

Fig. 3. The performance curves of WiDetect for one link.

Table 2. Detection Index (DI) for Different Regions

Region	R. #1	R. #2	R. #3	R. #4	R. #5
DI	0.52	0.22	0	0	0
Region	R. #6	A. #1	A. #2	A. #3	A. #4
DI	1	0.90	0.93	0.75	0.95

4.1. Validation of the Theoretical Analysis

We first verify the theoretical analysis described in Section 3. The Tx and Rx of WiDetect are placed in a typical office environment as shown in Fig. 2(a). One subject first walks around in the conference room for 30 minutes, and then walks in the area outside the conference room but within the square $ABCD$ for another 30 minutes, during the entire period of which the CSI data is collected. We also collect a set of one-hour CSI data when the environment is static.

We calculate the false alarm probability using the experimental CSI data and compare with the theoretical false alarm probability according to 8, and the comparison is shown in Fig. 3(a) for different sample sizes T and varying η. The theoretical curves match well with the experimental ones when η is greater, and the gap at smaller η is due to the correlation among different subcarriers, which we assume not existing in the theoretical analysis. In addition, the ROC curves in Fig. 3(b) show that the performance of WiDetect improves as T increases.

4.2. Coverage Test

In this experiment, to test the coverage of WiDetect, one subject walks in different regions of a single house as shown in Fig. 2(b) and the positions of the Tx and Rx are also indicated in the floorplan. We define the detection index (DI) of a region as the ratio between the duration when motion is detected and the total time when motion is present in that region. The results are summarized in Tab. 2. The motion occurring in Room #3–#5 cannot be detected since they are far away from the transmission devices. In some regions such as Room #1 and #2, motion is not detected all the time. However, as long as there is at least one motion detected along the subject's moving trajectory, the presence of that moving subject can be detected.

Table 3. Detection Index (DI) for Different Routes

Route	#1	#2	#3	#4
DI	0.90	0.98	0.83	1

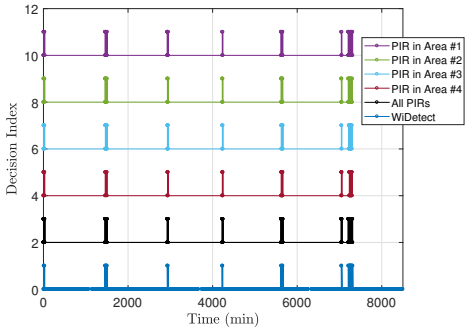

Fig. 4. Experimental results for long-term test compared with PIRs.

4.3. Intrusion Test

In this experiment, one subject tries to "break" into the house following four different routes as indicated in Fig. 2(b), and then leaves the house following the same route. The subject spends about one minute in the house for each route. The detection index for the four routes are shown in Tab. 3. The results show that the presence of the "intruder" can be detected most of the time for all the routes.

4.4. Long-Term Test

To evaluate the false alarm rate, we run WiDetect in the same single house for one week and compare with the detection that deploys 4 PIRs in different areas of the house. The detection results for both WiDetect and the four PIRs are shown in Fig. 4, where an even decision index (0, 2, 4, 6, 8, 10) indicates that no motion is detected. The results show that WiDetect can achieve comparable detection performance as the PIRs while having a much larger coverage.

5. CONCLUSIONS

In this work, we propose WiDetect, a highly accurate and calibration-free motion detection system leveraging CSI of a wireless channel. Extensive experiments show its superiority over existing motion detection approaches. Due to its large coverage, robustness, low cost, and low computational complexity, WiDetect is a very promising candidate for indoor motion detection applications.

6. REFERENCES

[1] Liang Wang, Guoying Zhao, Li Cheng, and Matti Pietikäinen, *Machine learning for vision-based motion analysis: Theory and techniques*, Springer, 2010.

[2] Ahmed E Kosba, Ahmed Saeed, and Moustafa Youssef, "Rasid: A robust wlan device-free passive motion detection system," in *Proc. of IEEE International Conferentce on Pervasive computing and communications*. IEEE, 2012, pp. 180–189.

[3] Yan Wang, Jian Liu, Yingying Chen, Marco Gruteser, Jie Yang, and Hongbo Liu, "E-eyes: Device-free location-oriented activity identification using fine-grained wifi signatures," in *Proc. of the 20th Annual International Conference on Mobile Computing & Networking*. 2014, pp. 617–628, ACM.

[4] Jiang Xiao, Kaishun Wu, Youwen Yi, Lu Wang, and Lionel M Ni, "Pilot: Passive device-free indoor localization using channel state information," in *Proc. of IEEE International Conference on Distributed Computing Systems (ICDCS)*. IEEE, 2013, pp. 236–245.

[5] Wei Wang, Alex X. Liu, Muhammad Shahzad, Kang Ling, and Sanglu Lu, "Understanding and modeling of WiFi signal based human activity recognition," in *Proc. of the 21st Annual International Conference on Mobile Computing & Networking*. 2015, pp. 65–76, ACM.

[6] Kun Qian, Chenshu Wu, Zheng Yang, Yunhao Liu, and Kyle Jamieson, "Widar: Decimeter-level passive tracking via velocity monitoring with commodity wi-fi," in *Proc. of the 18th ACM International Symposium on Mobile Ad Hoc Networking and Computing*. ACM, 2017, p. 6.

[7] Zimu Zhou, Zheng Yang, Chenshu Wu, Longfei Shangguan, and Yunhao Liu, "Omnidirectional coverage for device-free passive human detection," *IEEE Transactions on Parallel and Distributed Systems*, vol. 25, no. 7, pp. 1819–1829, 2014.

[8] Chenshu Wu, Zheng Yang, Zimu Zhou, Xuefeng Liu, Yunhao Liu, and Jiannong Cao, "Non-invasive detection of moving and stationary human with wifi," *IEEE Journal on Selected Areas in Communications*, vol. 33, no. 11, pp. 2329–2342, 2015.

[9] Jiguang Lv, Wu Yang, Liangyi Gong, Dapeng Man, and Xiaojiang Du, "Robust wlan-based indoor fine-grained intrusion detection," in *Proc. of IEEE Global Communications Conference (GLOBECOM)*. IEEE, 2016, pp. 1–6.

[10] Tzi-Dar Chiueh, Pei-Yun Tsai, and I-Wei Lai, *Baseband receiver design for wireless MIMO-OFDM communications*, John Wiley & Sons, 2012.

[11] C. Chen, Y. Chen, Y. Han, H. Q. Lai, F. Zhang, and K. J. R. Liu, "Achieving centimeter-accuracy indoor localization on WiFi platforms: A multi-antenna approach," *IEEE Internet of Things Journal*, vol. 4, no. 1, pp. 122–134, Feb 2017.

[12] Souvik Sen, Božidar Radunovic, Romit Roy Choudhury, and Tom Minka, "You are facing the Mona Lisa: Spot localization using PHY layer information," in *Proc. of the 10th International Conference on Mobile Systems, Applications, and Services*. 2012, pp. 183–196, ACM.

[13] David A Hill, *Electromagnetic fields in cavities: deterministic and statistical theories*, vol. 35, John Wiley & Sons, 2009.

[14] George EP Box, Gwilym M Jenkins, Gregory C Reinsel, and Greta M Ljung, *Time series analysis: forecasting and control*, John Wiley & Sons, 2015.